PHILOSOPHICAL TRANSACTIONS OF THE ROYAL SOCIETY A MATHEMATICAL, PHYSICAL & ENGINEERING SCIENCES

A Laboratory Study of Melt Migration

M. J. Daines and D. L. Kohlstedt

Phil. Trans. R. Soc. Lond. A 1993 **342**, 43-52
doi: 10.1098/rsta.1993.0003

A laboratory study of melt migration

By M. J. Daines and D. L. Kohlstedt

Department of Geology and Geophysics, University of Minnesota, Pillsbury Hall, Minneapolis, Minnesota 55455, U.S.A.

Melt migration experiments have been carried out to investigate the dependence of permeability on melt fraction and on orthopyroxene content for partly molten aggregates of olivine plus basalt and olivine-orthopyroxene plus basalt. Melt migration couples, formed between discs of olivine or olivine with 20 vol % orthopyroxene plus *ca.* 8 vol % basalt and discs with either *ca.* 2 vol % or 0 vol % basalt, were heated at 1250 °C and 300 MPa for 6–32 h. The resulting melt migration profiles, which developed in response to capillary forces, were analysed in terms of coupled differential equations describing melt migration via porous flow through a deformable matrix (compaction theory). For the experiments in which melt was initially present in both the source and the sink, the melt migration profiles could be fit equally well with a permeability proportional to the melt fraction to the first, second or third power. For the experiments in which the sink initially was melt-free, a best fit to the melt migration profiles could be obtained with a permeability that is linearly proportional to melt fraction. The melt migration profiles for samples in which the sink disc contained olivine plus 20 vol % orthopyroxene were essentially identical to those for samples in which the sink contained only olivine, even though at least some of the triple junctions in the former samples were not wetted by the melt phase.

1. Introduction

The rate at which melt percolates through partly molten regions of the mantle affects both the chemical composition and the physical properties of the host rock (cf. Richter & McKenzie 1984; McKenzie 1989; Kohlstedt 1992). In a rock undergoing pressure-release melting beneath a mid-ocean ridge, for example, the melt fraction will increase with increasing degree of melting, if the permeability is low. Such an increase in melt fraction could result in a marked decrease in viscosity (van der Molen & Paterson 1979). In contrast, if the permeability is relatively high such that the melt fraction remains low (e.g. below *ca.* 5 vol %), then the melt will have very little effect on the rheological behaviour of the partly molten rock (Cooper & Kohlstedt 1986; Cooper *et al.* 1989).

The ability to establish an interconnected melt network in partly molten rocks is a prerequisite for melt transport by porous flow and depends on the grain-scale distribution of melt. Melt distribution can be characterized by the dihedral angle, which is a function of the relative values of the solid–solid and solid–melt interfacial energies in the rock. In mantle analogues composed of olivine plus silicate melt, reported dihedral angles range from 20 to *ca.* 50° (cf. Waff & Bulau 1979, 1982;

Phil. Trans. R. Soc. Lond. A (1993) **342**, 43–52
Printed in Great Britain

Toramaru & Fujii 1986), implying that silicate melt in an olivine matrix is completely interconnected with melt confined to three and four grain junctions (Smith 1964; Beere 1975; Wray 1976; Bulau *et al.* 1979). This interpretation of these values for the dihedral angle has been experimentally confirmed (Vaughan *et al.* 1982; Daines & Richter 1988; Kohlstedt 1990). The upper mantle, although composed predominantly of olivine, also contains other crystalline phases, such as orthopyroxene, which may affect the establishment of an interconnected melt network. Microstructural studies of partly molten peridotites (Toramaru & Fujii 1986; Fujii *et al.* 1986; von Bargen & Waff 1988) suggest that, depending on water content, dihedral angles of melt in contact with orthopyroxene could be significantly higher than those for basalt in contact with olivine, potentially resulting in imperfect melt connectivity and a reduction in permeability (Toramaru & Fujii 1986; Nakano & Fujii 1989).

In an earlier series of experiments designed to investigate the kinetics of melt migration in aggregates of olivine plus a silicate melt, melt was induced to flow from a melt-rich source to a melt-free sink in response to the capillary forces arising from the gradient in melt fraction (Watson 1982; Riley & Kohlstedt 1990; Riley & Kohlstedt 1992). To determine a permeability as a function of melt fraction, the resulting melt migration profiles were analysed in terms of the compaction theory that was developed to describe porous flow through a deformable matrix (McKenzie 1984), but modified to replace buoyancy with a capillary driving force (Riley *et al.* 1990; Riley & Kohlstedt 1991). One striking and unanticipated result of these studies was a linear dependence of permeability, K, on melt fraction, ϕ (i.e. $K \propto \phi^1$). In contrast, permeability models yield power-law relations between permeability and melt fraction of the form

$$K(\phi) = (d^2/b)\,\phi^n \tag{1}$$

with $2 \leqslant n \leqslant 3$ (Turcotte & Schubert 1982, pp. 383–384; McKenzie 1984; Dullien 1992, ch. 3). In equation (1), d is the grain size and b is a geometrical constant. In particular, Cheadle (reported in McKenzie (1989)) analysed the permeability of a melt–solid system for which the pore geometry is texturally equilibrated (i.e. determined by the relative values of the solid–solid and solid–melt interfacial energies (cf. von Bargen & Waff 1986)); this analysis yielded $n = 2$ for $\phi < 0.03$ and $n = 3$ for $\phi > 0.03$.

For melt migration experiments in which the sink for melt initially is free of melt, one complication in applying a continuum formalism such as compaction theory is associated with the form of the capillary driving force

$$\frac{\partial}{\partial z}\left(-\frac{\partial G_{\mathrm{v}}}{\partial \phi}\right) = \frac{\gamma_{\mathrm{sm}} H(\theta)}{\sqrt{3}d}\,\frac{1}{\phi^{\frac{3}{2}}}\,\frac{\partial \phi}{\partial z}, \tag{2}$$

where G_{v} is the free energy per unit volume associated with the presence of solid–solid and solid–melt interfaces, γ_{sm} is the solid melt interfacial energy, $H(\theta)$ is a function of the dihedral angle θ (cf. Riley & Kohlstedt 1991), and z is the spatial coordinate in the direction of melt flow. Based on equation (2), the driving force for melt migration approaches infinity as the melt fraction in the sink goes to zero.

Hence in the present study, two series of experiments were undertaken, one to eliminate the complication associated with a melt-free sink and the other to explore the effect of enstatite on the kinetics of melt migration. In the first set of experiments, melt migration couples were prepared in which not only the source, but

PHILOSOPHICAL TRANSACTIONS OF THE ROYAL SOCIETY A MATHEMATICAL, PHYSICAL & ENGINEERING SCIENCES

Table 1. *Composition of melt and crystalline phases used in melt migration experiments*

oxide component	MORB[a] (wt %)	Alkali basalt[b] (wt %)	Balsam Gap dunite[a] (wt %)	Bamble enstatite (wt %)	San Carlos olivine (wt %)
SiO_2	50.02	46.5	40.5	56.2	39.66
MgO	9.09	8.7	51.1	32.4	51.1
FeO	9.24	12.4	7.51	9.7	9.1
CaO	11.51	9.9	0.01	0.2	0.14
Al_2O_3	15.63	14.9	—	0.07	0.07
Na_2O	3.12	3.0	—	0	0.01
K_2O	0.27	0.97	—	0.07	—
TiO_2	1.55	0.97	—	0.07	—
P_2O_5	0.21	2.4	—	0.05	—
Cr_2O_3	0.05	0.3	—	—	—
NiO	—	—	0.31	—	—

[a] Cooper & Kohlstedt (1984).
[b] Helz (1973).

also the sink contained melt; the melt fraction in the sink was about one-fifth that in the source. In the second set of experiments, the crystalline matrix was composed of olivine plus orthopyroxene. The resulting melt migration profiles from both types of experiments were analysed in terms of compaction theory to determine the dependence of permeability on melt fraction.

2. Experimental procedure

Melt migration couples for the two different types of experiments were formed by pressing together two polycrystalline discs, one a source for melt and the other a sink for melt. In the first set of experiments, both source and sink discs were composed of olivine plus alkali basalt to determine the dependence of permeability on melt fraction. Source discs contained *ca.* 8 vol % melt and the sink discs *ca.* 2 vol % melt. In the second set of experiments, source discs were composed of dunite with *ca.* 20 vol % enstatite plus basalt, whereas sink discs were melt-free containing either olivine or dunite plus *ca.* 20 vol % enstatite to investigate the effect of orthopyroxene on the kinetics of melt migration. All discs were separately fabricated by isostatically hot-pressing mechanical mixtures of powders of the appropriate composition. Starting powders with a particle size of less than 10 μm were obtained by mechanically grinding San Carlos olivine, Balsam Gap dunite, Bamble enstatite, a mid-ocean ridge basalt (MORB) and an alkali basalt. Because the powers used in our experiments were dried at only 150 °C, compaction and melt migration most likely occurred under 'wet' conditions. Compositions of starting materials are listed in table 1.

To synthesize texturally and chemically equilibrated source and sink discs with a density of 99 % of the theoretical value, each disc was held at *ca.* 1250 °C for at least 3 h at 300 MPa confining pressure in a gas-medium high-pressure vessel. The discs were jacketed in Ni to control the oxygen partial pressure within the olivine stability field at the Ni–NiO phase boundary. For the melt migration experiments, each melt migration couple (encapsulated in Ni) was held at *ca.* 1250 °C, 300 MPa for between

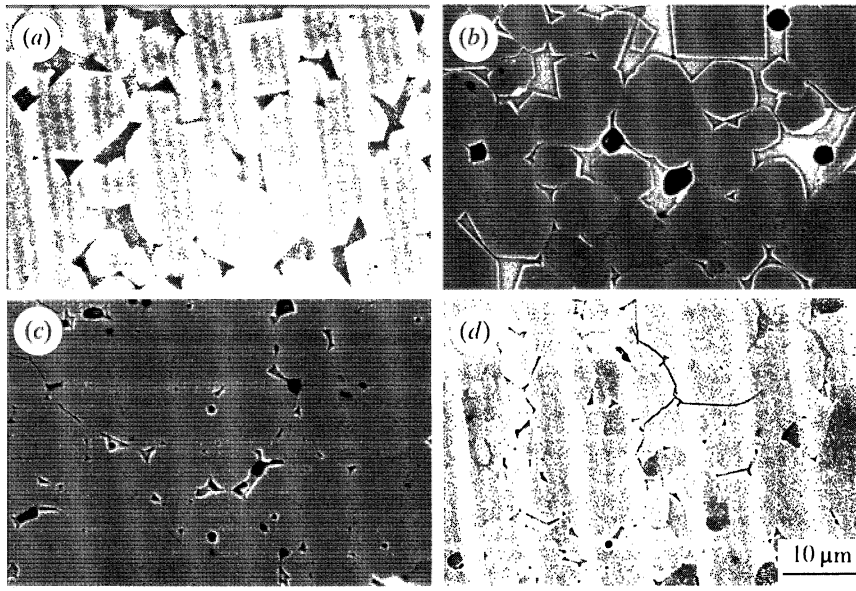

Figure 1. SEM micrographs of typical microstructures in melt migration couples. Glass appears as darker grey regions, although the central portion of larger glass pockets in back-scattered electron images (*b*), (*c*) and (*d*) are very light. Olivine is light grey; orthopyroxene is an intermediate grey. The darkest regions are pores or small cracks in the sample. (*a*) Secondary electron image of the source region in the 32 h olivine–alkali basalt melt migration experiment. (*b*) Back-scattered electron image of the source region in the ol–opx–MORB experiment. (*c*) Back-scattered image of the sink that initially contained only olivine in the ol–opx–MORB experiment. (*d*) Back-scattered electron image of the sink that initially contained olivine and orthopyroxene in the ol–opx–MORB experiments.

6 and 32 h. The couples, each *ca.* 7 mm in diameter and *ca.* 2 mm in length, were then cut normal to the interface between the source and the sink discs and polished to a 0.05 μm finish.

Median dihedral angles were determined by a statistical analysis of 250 measurements of triple junctions on scanning electron microscope (SEM) micrographs. Grain diameters were measured on an optical microscope as well as on SEM micrographs; at least 100 measurements were made to determine mean grain sizes for source and sink discs. Melt migration profiles were subsequently obtained with an image analysis system associated with the SEM.

Each melt migration profile was analysed in terms of compaction theory for porous flow through a deformable matrix (McKenzie 1984), modified by replacing the buoyancy driving force with a capillary driving force (Riley & Kohlstedt 1991). A comparison of the experimentally determined melt migration profiles with those generated from simulations based on compaction theory yielded values for the compaction length, δ_c, and the characteristic time, τ_0. These fitting parameters are related to the permeability at the starting melt fraction in the source, K_0, the viscosity of the partly molten rock, η_{pm}, and the viscosity of the melt, μ, as well as d, $H(\theta)$ and γ_{sm}:

$$\delta_c = (K_0\,\eta_{pm}/\mu)^{\frac{1}{2}}, \tag{3}$$

$$\tau_0 = \sqrt{3}\,d\eta_{pm}/\gamma_{sm}\,H(\theta). \tag{4}$$

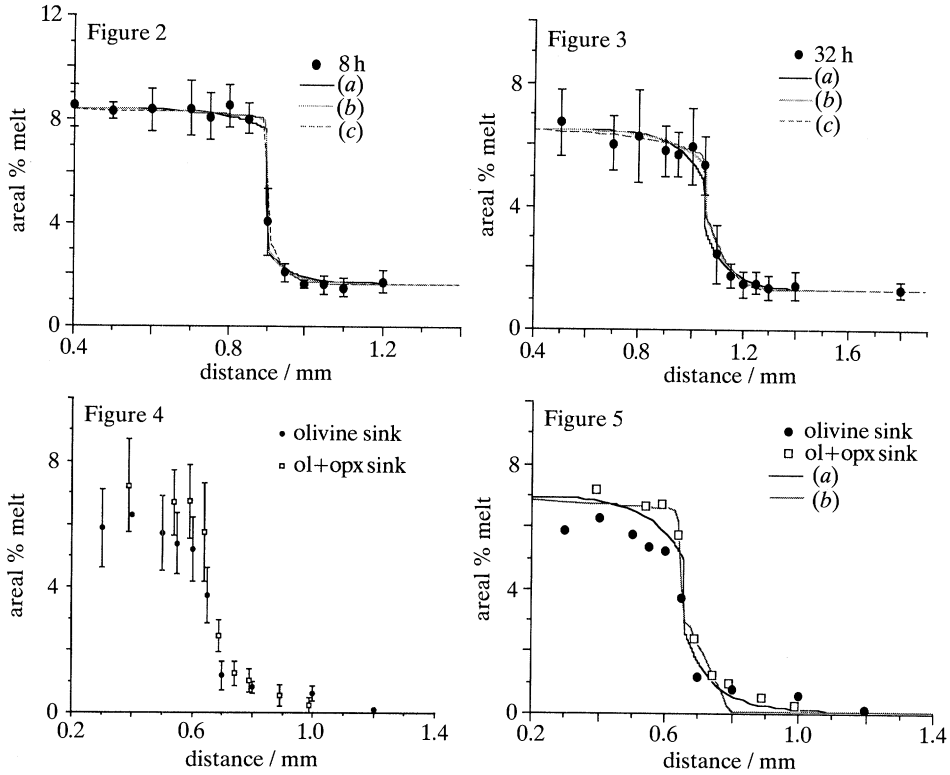

Figure 2. Plot of the melt fraction profile and final melt distributions from best-fit simulations for $n = 1$, 2 and 3 for the 8 h olivine plus alkali basalt experiment in which the sink initially contained some melt. (*a*) $n = 1$, $\delta_c = 90$ μm; (*b*) $n = 2$, $\delta_c = 150$ μm; (*c*) $n = 3$, $\delta_c = 200$ μm.

Figure 3. Plot of the melt fraction profile and final melt distributions from best-fit simulations for $n = 1$, 2 and 3 for the 32 h olivine plus alkali basalt experiment in which the sink originally contained some melt. (*a*)–(*c*) As for figure 2.

Figure 4. Plot of the melt fraction profiles for olivine–orthopyroxene–MORB experiments in which one sink contained only olivine and the other contained only olivine plus orthopyroxene (i.e. the sinks were initially melt-free).

Figure 5. Plot of the melt fraction profiles for olivine–orthopyroxene–MORB experiments and final melt distributions from best-fit simulations for $n = 1$ and 3. (*a*) $n = 1$, $\delta_c = 150$ μm; (*b*) $n = 3$, $\delta_c = 500$ μm.

3. Results

Typical microstructures of samples are shown in figure 1. Both large glass pockets and small triangular triple junctions are present in all samples; the frequency and size of the large glass pockets decreases as glass fraction decreases. Olivine (ol) and orthopyroxene (opx) grains in contact with larger glass pockets tend to be faceted; as the size of the glass pockets decreases, these interfaces become more smoothly curved. All of the triple junctions that were examined in samples containing only olivine appear to contain some glass. In samples containing orthopyroxene, however, some triple junctions in which orthopyroxene is present appear to be glass-free. It is important to note that glass pockets smaller than 0.01 μm are not detectable because of the resolution of the imaging methods used. Similar microstructures have also been described by von Bargen & Waff (1988). Grain size increased in all

Table 2. *Parameters obtained from melt migration experiments at* 1250 °C *with a sink of olivine plus* 2 *vol* % *basalt*

$\frac{t}{10^4\ \mathrm{s}}$	n	$\frac{\tau_0}{10^6\ \mathrm{s}}$	$\frac{\delta_c}{\mu\mathrm{m}}$	$\frac{\eta_{pm}}{(10^{10}\ \mathrm{Pa\ s})}$	$\frac{K_0}{(10^{-18}\ \mathrm{m}^2)}$	$\frac{d_0}{\mu\mathrm{m}}$	$\frac{d_f^{src}}{\mu\mathrm{m}}$	$\frac{d_f^{snk}}{\mu\mathrm{m}}$
2.88	1	11.52	90	9.6	0.84	9,0	10.5	10.5
	2		150		2.3			
	3		200		4.2			
11.52	1	11.52	90	6.3	1.3	9	13.5	16.5
	2		150		3.6			
	3		200		6.3			

Table 3. *Parameters obtained using* $n = 1$ *from melt migration experiments at* 1250 °C *with a sink of olivine or olivine plus* 20 *vol* % *orthopyroxene*

sink material	$\frac{t}{10^4\ \mathrm{s}}$	$\frac{\tau_0}{10^6\ \mathrm{s}}$	$\frac{\delta_c}{\mu\mathrm{m}}$	$\frac{\eta_{pm}}{10^{10}\ \mathrm{Pa\ s}}$	$\frac{K_0}{10^{-18}\ \mathrm{m}^2}$	$\frac{d_0}{\mu\mathrm{m}}$	$\frac{d_f^{src}}{\mu\mathrm{m}}$	$\frac{d_f^{snk}}{\mu\mathrm{m}}$
ol + opx	2.16	4.32	200	4.6	8.7	9.0	11.4	9.3
		2.88	150	3.0	7.5			
		2.16	100	2.2	4.5			
ol	2.16	8.64	200	7.7	5.2	9.0	13.5	13.5
		4.32	150	3.9	5.8			
		2.88	100	2.6	3.8			

samples during the melt migration experiments (see tables 2 and 3). The median dihedral angle for ol–ol–alkali basalt contacts was *ca.* 38°; for ol–ol–MORB, 27°; for ol–opx–MORB, 34°; for opx–opx–MORB, 41°. The median angle reported for opx–opx–MORB contacts is based on only 45 measurements due to the relative scarcity of these contacts.

Melt migration profiles, plotted as areal percent melt against distance in figures 2–5, illustrate that melt is transported from the source into the sink in all experiments. Within experimental uncertainties, the decrease in the amount of melt in the source is equal to the increase in the amount in the sink. Comparison of figure 2 with figure 3 demonstrates that the amount of melt that migrates from the source into the sink during an experiment increases with increasing time. The effect of the addition of orthopyroxene on the extent of melt migration is illustrated in figure 4.

Also presented in figures 2, 3 and 5 are the melt migration profiles obtained from compaction theory for values of $n = 1$, 2 and 3, where n is defined in equation (1) (i.e. $K \propto \phi^n$). For the experiments in which the sink initially contained some melt, the values of the parameters used to non-dimensionalize the compaction equations are summarized for each value of n in table 2. Values for the K_0 and η_{pm}, calculated from equations (3) and (4) using $\mu = 10$ Pa s (Ryan & Blevins 1987) and $\gamma_{sm} = 0.5$ J m^{-2} (Cooper & Kohlstedt 1982), are also listed. In tables 2 and 3, d_0, d_f^{src} and d_f^{snk} are the starting grain size in the melt migration couple, the final grain size in the source disc and the final grain size in the sink disc, respectively.

For the experiments in which the sink initially was melt-free, the values of the parameters used to non-dimensionalize the compaction equations are summarized in table 3. Because $n = 1$ clearly provides the best fit for these experiments (figure 5), only the values of the non-dimensionalization parameters obtained when $n = 1$ are

reported. Again, values of $\mu = 10$ Pa s and $\gamma_{sm} = 0.5$ J m^{-2} were used to calculate K_0 and η_{pm} for these experiments.

4. Discussion

(*a*) *Effect of a melt-bearing sink*

Based on these experiments it is not possible to determine the dependence of permeability on melt fraction, except in those experiments in which the sink did not initially contain melt. As seen in figures 2 and 3, the experimental data can be fitted equally well with $n = 1$, 2 or 3. In part this lack of sensitivity in these experiments to the value of n could have been anticipated. Since $K \propto \phi^n$, the larger the value of ϕ, the smaller the order of magnitude change in permeability as n increases. In other words, as the melt fraction increases, the model and hence the experiment become insensitive to the difference in permeability that results from choosing different values of n. Consequently, it is only at very small melt fractions that the choice of n greatly affects the shape of the melt migration profile. In figures 2 and 3 it is apparent that even in the case of perfect sample homogeneity and errorless analysis, it would be difficult to determine a unique value of n. It is still possible, however, to extract information about the kinetics of melt migration from these experiments.

Because the scaling parameter τ_0 does not depend on the choice of n, the viscosity of the partially molten sample η_{pm} can be determined. The values obtained for the experiments run for 8 and 32 h, 9.6×10^{10} and 6.3×10^{10} Pa s, respectively, compare well to the viscosity of *ca.* 1×10^{11} Pa s for 'wet', partly molten olivine deforming by grain boundary diffusional creep at 1250 °C for a grain size of *ca.* 10 μm (Karato 1986; Cooper *et al.* 1989; Kohlstedt & Chopra 1993). The difference between the values for η_{pm} determined for the two experiments arises because, in fitting the data with the numerical simulations it was assumed that the time scaling parameter τ_0 should be constant for both experiments. Since $\eta_{pm} \propto \tau_0/d$ (equation (4)), the difference in the final mean grain size between the samples results in a small difference in η_{pm}, with the sample with the larger grain size having the lower viscosity. In fact, because for $\eta_{pm} \propto d^3$ in the grain boundary diffusion creep régime (Rutter 1976), it is likely that the matrix in the 32 h experiment, which had a larger final grain size, was more viscous than the matrix in the 8 h experiment. Even though this dependence of viscosity on grain size introduces some uncertainty into the determination of η_{pm}, it will not likely affect the value by more than a factor of 2.

Although the value of η_{pm} obtained is not dependent on the value of n, the value of K_0 increases by a factor of 5 as n is increased from 1 to 3. However, this variation is small compared to the discrepancy between the average value for K_0 obtained in our study, *ca.* 3×10^{-18} m^2, and that determined by Riley *et al.* (1990) and Riley & Kohlstedt (1991), *ca.* 2×10^{-15} m^2. One of the differences between the present experiments and the earlier experiments is the initial presence of melt in the sink disc. This difference, however, can not explain the discrepancy, because the values for K_0, *ca.* 4 to 8×10^{-18} m^2, obtained in the ol–opx–MORB experiments, in which the sink initially contained no melt, are also significantly smaller than those of Riley *et al.* (1990) and Riley & Kohlstedt (1991). The major uncertainty in calculating K_0 – and hence the likely source of the discrepancy – is in the values used for the viscosity of the melt phase μ. In the earlier experiments, the silicate melt was rich in potassium and aluminium; in the present experiments, the potassium content was

almost negligible and the aluminium content was about a factor of two smaller. In both cases, values for μ were calculated from published compilations of melt viscosity (Ryan & Blevins 1987); consequently, uncertainties in these values could be large. Independent measurements of the viscosity of the melt phases are clearly needed.

The implications of the much smaller K_0 determined in the present experiments can be illustrated by calculating the length scale over which melt segregation via porous flow will be rapid enough to maintain the low resident melt fraction of 0.1 % which was calculated by Riley *et al.* (1990). It was assumed in the original calculations that the melt production rate in a 50 km melting column under a mid-ocean ridge is equal to the melt extraction rate and that permeability is linearly dependent on melt fraction. Using the same melt production rate and requiring that the resident melt fraction be 0.1 %, substitution of the permeability obtained in the present study for those of Riley *et al.* (1990) gives a length scale of *ca.* 20 m over which porous flow will occur rapidly enough to keep the melt fraction low. This length scale can be increased by either allowing the resident melt fraction to be higher or by decreasing the melt production rate. The implication of this smaller length scale over which porous flow is an effective mechanism of melt segregation is that there must be a transition from porous to channelized flow in the mantle on a comparable length scale.

(*b*) *Effect of the addition of orthopyroxene*

The addition of orthopyroxene does not have a substantial effect on the kinetics of melt migration; at most, there may be a very slight enhancement in the melt migration rate for samples containing orthopyroxene (figure 4). Microstructural evidence would suggest, however, that melt migration should actually be retarded in samples containing orthopyroxene due to the presence of some melt-free triple junctions (figure 1), which should increase the tortuosity of melt migration paths and consequently reduce the permeability. Toramaru & Fujii (1986) predicted that, in rocks in which olivine and orthopyroxene grain sizes are similar, complete melt connectivity is not obtained once the orthopyroxene content exceeds 25 vol %. In our experiments, the grain sizes of olivine and orthopyroxene are approximately equal, so that the presence of 20 % orthopyroxene may not be sufficient to produce a measurable effect on the permeability. In addition, Toramaru & Fujii's analysis was based on a dihedral angle of 76° for opx–opx–melt in a dry peridotite; the dihedral median angle for opx–opx–melt contacts was *ca.* 41° (excluding melt-free triple junctions) in the present study for apparently wet samples. (Note that it has previously been observed (Fujii *et al.* 1986; von Bargen & Waff 1988) that the presence of water reduces the dihedral angle between orthopyroxene and basalt.)

The viscosities for the partly molten aggregates determined from the melt migration profiles for the olivine and the olivine plus orthopyroxene samples are the same within error. This result is consistent with limited data that are available for comparison of the rheology of olivine and olivine plus orthopyroxene aggregates (Hitchings & Paterson 1989).

Finally, it should be emphasized that the best fit of the coupled differential equations describing compaction theory to the experimental melt migration profiles for the experiments in which the sink initially was melt-free yields $n = 1$ (i.e. $K \propto \phi^1$). This result thus confirms that previously reported by Riley *et al.* (1990) and Riley & Kohlstedt (1991). Model calculations using compaction theory demonstrate that if our new sample design in which both the source and the sink initially contain melt

is to be used to constrain the value of n, then the melt fraction in the sink must be less than about one-tenth that in the source. These experiments are presently in progress in our laboratory.

Support from the National Science Foundation through grant EAR-8916438 is gratefully acknowledged.

References

Beere, W. 1975 A unifying theory of the stability of penetrating liquid phases and sintering pores. *Acta metall.* **23**, 131–138.

Bulau, J. R., Waff, H. S. & Tyburczy, J. A. 1979 Mechanical and thermodynamic constraints on fluid distribution in partial melts. *J. geophys. Res.* **84**, 6102–6108.

Cooper, R. F. & Kohlstedt, D. L. 1982 Interfacial energies in the olivine-basalt system. In *Advances in Earth and planetary sciences* (ed. S. Akimoto & M. H. Manghnani), vol. 12 (*High Pressure Research in Geophysics*), pp. 217–228. Tokyo: Center for Academic Publications.

Cooper, R. F. & Kohlstedt, D. L. 1984 Sintering of olivine and olivine-basalt aggregates. *Phys. Chem. Minerals* **11**, 5–16.

Cooper, R. F. & Kohlstedt, D. L. 1986 Rheology and structure of olivine-basalt partial melts. *J. geophys. Res.* **91**, 9315–9323.

Cooper, R. F., Kohlstedt, D. L. & Chyung, K. 1989 Solution-precipitation enhanced creep in solid–liquid aggregates which display a non-zero dihedral angle. *Acta metall.* **37**, 1759–1771.

Daines, M. J. & Richter, F. M. 1988 An experimental method for directly determining the interconnectivity of melt in a partially molten system. *Geophys. Res. Lett.* **15**, 1459–1462.

Helz, R. T. 1973 Phase relations of basalts in their melting range at $P_{H_2O} = 5$ kb as a function of oxygen fugacity. *J. Petrol.* **14**, 249–302.

Hitchings, R. S., Paterson, M. S. & Bitmead, J. 1989 Effects of iron and magnetite additions in olivine-pyroxene rheology. *Phys. Earth planet. Interior* **55**, 277–291.

Karato, S.-I., Paterson, M. S. & FitzGerald, J. D. 1986 Rheology of synthetic olivine aggregates: Influence of grain size and water. *J. geophys. Res.* **91**, 8151–8176.

Kohlstedt, D. L. 1990 Chemical analysis of grain boundaries in an olivine–basalt aggregate using high-resolution, analytical electron microscopy. In *The brittle–ductile transition in rocks: the Heard volume* (ed. A. G. Duba, W. B. Durham, J. W. Handin & W. F. Wang), pp. 211–218. Washington: American Geophysical Union.

Kohlstedt, D. L. 1992 Structure, rheology and permeability of partially molten rocks at low melt fractions. In *Mantle flow and melt generation at mid-ocean ridges* (ed. J. P. Morgan), 1990 vol. (*RIDGE Summer Institute*). Washington: American Geophysical Union.

Kohlstedt, D. L. & Chopra, P. N. 1993 Influence of basaltic melt on the creep of polycrystalline olivine under hydrous conditions. In *Magmatic systems* (ed. M. P. Ryan). New York: Academic Press.

McKenzie, D. 1984 The generation and compaction of partially molten rock. *J. Petrol.* **25**, 713–765.

McKenzie, D. 1989 Some remarks on the movement of small melt fractions in the mantle. *Earth planet. Sci. Lett.* **95**, 53–72.

Nakano, T. & Fujii, N. 1989 The multiphase grain control percolation: its implication for a partially molten rock. *J. geophys. Res.* **94**, 15,653–15,661.

Ribe, N. M. 1987 Theory of melt segregation – a review. *J. Volcan. geotherm. Res.* **33**, 241–253.

Richter, F. M. & McKenzie, D. 1984 Dynamical models for melt segregation from a deformable matrix. *J. Geol.* **92**, 729–740.

Riley, G. N. Jr & Kohlstedt, D. L. 1990 An experimental study of melt migration in an olivine–melt system. In *Magma transport and storage* (ed. M. P. Ryan), pp. 77–86. New York: Wiley.

Riley, G. N. Jr & Kohlstedt, D. L. 1991 Kinetics of melt migration in upper mantle-type rocks. *Earth planet. Sci. Lett.* **105**, 500–521.

Riley, G. N. Jr, Kohlstedt, D. L. & Richter, F. M. 1990 Melt migration in a silicate liquid–olivine system: an experimental test of compaction theory. *Geophys. Res. Lett.* **17**, 2101–2104.

PHILOSOPHICAL TRANSACTIONS OF THE ROYAL SOCIETY A MATHEMATICAL, PHYSICAL & ENGINEERING SCIENCES

Riley, G. N. Jr & Kohlstedt, D. L. 1992 The influence of H_2O and CO_2 on melt migration in two silicate liquid-olivine systems. In *Fault mechanics and transport properties in rocks* (ed. B. Evans & T.-F. Wong) (*A Symposium in Honor of W. F. Brace*), pp. 281–293. New York: Academic Press.

Rutter, E. H. 1976 The kinetics of rock deformation by pressure solution. *Phil. Trans. R. Soc. Lond.* A **283**, 203–219.

Ryan, M. P. & Blevins, J. Y. K. 1987 *The viscosity of synthetic and natural silicate melts and glasses at high temperatures and* 1 bar (10^5 Pa) *pressure and at higher pressures.* (466 pages.) Denver: U.S. Geological Survey.

Smith, C. S. 1964 Some elementary principles of polycrystalline microstructure. *Metall. Rev.* **9**, 1–47.

Toramaru, A. & Fujii, N. 1986 Connectivity of melt phase in a partially molten peridotite. *J. geophys. Res.* **91**, 9239–9252.

van der Molen, I. & Paterson, M. S. 1979 Experimental deformation of partially melted granite. *Contrib. Mineral. Petrol.* **70**, 291–318.

Vaughan, P. J., Kohlstedt, D. L. & Waff, H. S. 1982 Distribution of the glass phase in hot-pressed, olivine–basalt aggregates: an electron microscopy study. *Contrib. Mineral. Petrol.* **81**, 253–261.

von Bargen, N. & Waff, H. S. 1986 Permeabilities, interfacial areas and curvatures of partially molten systems: results of numerical computations of equilibrium microstructures. *J. geophys. Res.* **91**, 9261–9276.

von Bargen, N. & Waff, H. S. 1988 Wetting of enstatite by basaltic melt at 1350 °C and 1.0- to 2.5-GPa pressure. *J. geophys. Res.* **93**, 1153–1158.

Waff, H. S. & Bulau, J. R. 1979 Equilibrium fluid distribution in an ultramafic partial melt under hydrostatic stress conditions. *J. geophys. Res.* **84**, 6109–6114.

Waff, H. S. & Bulau, J. R. 1982 Experimental determination of near-equilibrium textures in partially molten silicates at high pressures. In *Advances in Earth and planetary sciences* (ed. S. Akimoto & M. H. Manghnani), vol. 12 (*High Pressure Research in Geophysics*), pp. 229–236. Tokyo: Center for Academic Publications.

Watson, E. B. 1982 Melt infiltration and magma evolution. *J. Geol.* **10**, 236–240.

Wray, P. J. 1976 The geometry of two-phase aggregates in which the shape is determined by its dihedral angle. *Acta metall.* **24**, 125–135.

PHILOSOPHICAL TRANSACTIONS OF THE ROYAL SOCIETY A MATHEMATICAL, PHYSICAL & ENGINEERING SCIENCES

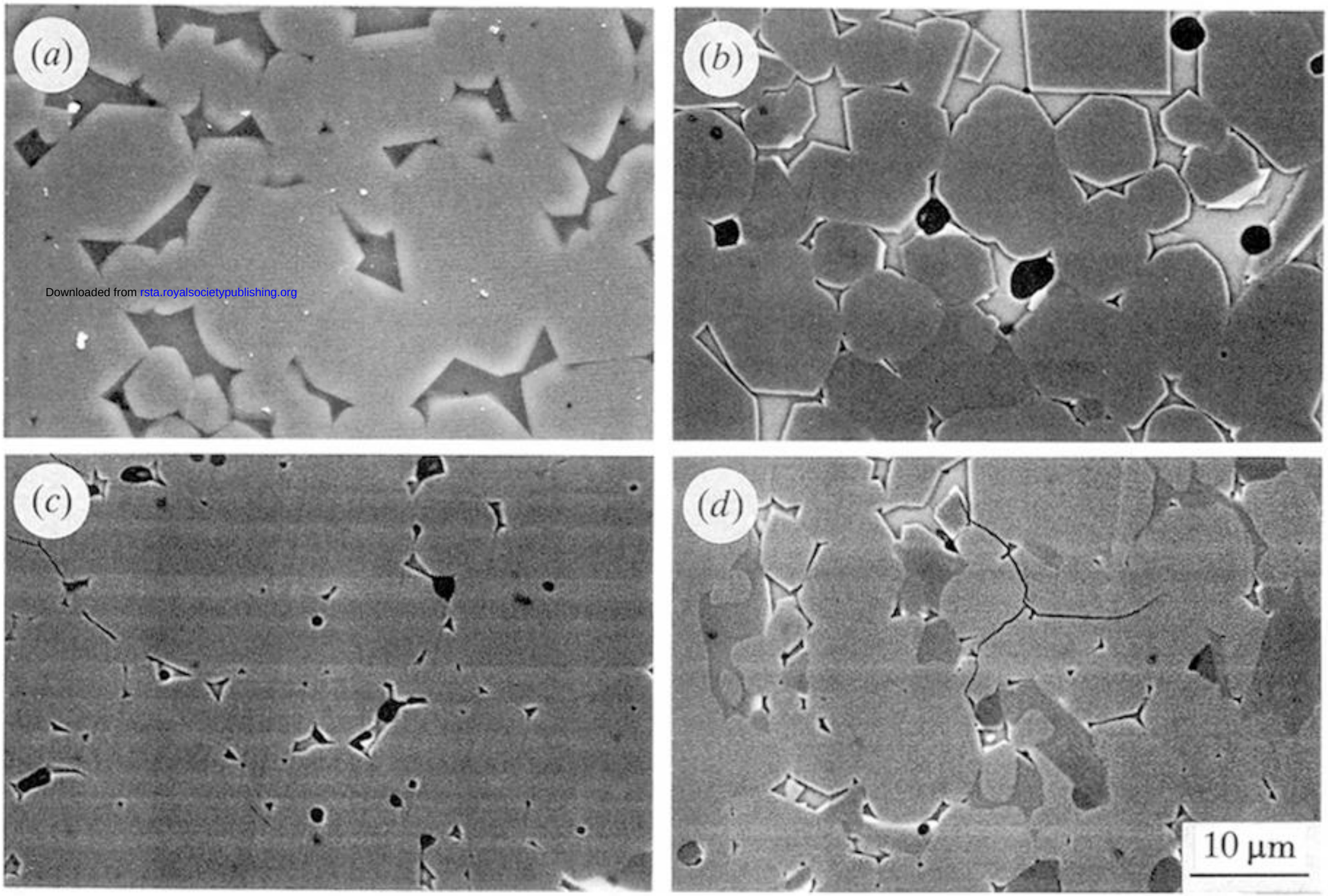

igure 1. SEM micrographs of typical microstructures in melt migration couples. Glass appears as arker grey regions, although the central portion of larger glass pockets in back-scattered electron nages (*b*), (*c*) and (*d*) are very light. Olivine is light grey; orthopyroxene is an intermediate grey. he darkest regions are pores or small cracks in the sample. (*a*) Secondary electron image of the ource region in the 32 h olivine–alkali basalt melt migration experiment. (*b*) Back-scattered ectron image of the source region in the ol–opx–MORB experiment. (*c*) Back-scattered image of the nk that initially contained only olivine in the ol–opx–MORB experiment. (*d*) Back-scattered ectron image of the sink that initially contained olivine and orthopyroxene in the ol–opx–MORB xperiments.